

Graphical Abstract

A Coupled Darcy-Richards Framework for Hydrological Modeling of Permeable Pavements, Green Roofs, and Bioretention Systems

Marcus Nóbrega Gomes Jr., Jose Artur Teixeira Brasil, Drew Johnson, Athanassios T. Papagianakis, Marcio Hofheinz Giacomoni

A Coupled Darcy-Richards Framework for Hydrological Modeling of Permeable Pavements, Green Roofs, and Bioretention Systems

Catchment-Scale Model

- Non-Linear Reservoir
- SCS-CN (adapted to continuous simulation)

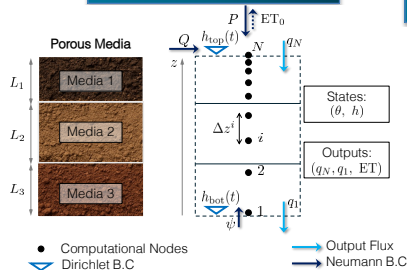
Mixed-Form 1D Richards

- Spatially-varied mesh
- Newton-Raphson Solver

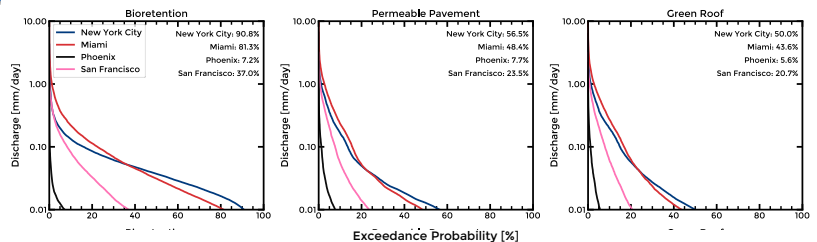
Model Evaluation

- Hydrus-1D Benchmarking
- Real-world Permeable Pavement (Calibration/Validation)
- 30-yr Continuous Simulation

Conceptual Model



30-yr Hydrologic Signatures of Bioretention Systems, Permeable Pavements, and Green Roofs (New York City, Miami, Phoenix, and San Francisco)



Highlights

A Coupled Darcy-Richards Framework for Hydrological Modeling of Permeable Pavements, Green Roofs, and Bioretention Systems

Marcus Nóbrega Gomes Jr., Jose Artur Teixeira Brasil, Drew Johnson, Athanassios T. Papagianakis, Marcio Hofheinz Giacomoni

- A coupled Darcy-Richards model simulates LID systems under climate variability
- Validation against Hydrus-1D resulted in $RMSE = 0.020m$ and 0.003 for water content
- Calibration to field-scale permeable asphalt resulted in $NSE = 0.93$ and $R^2 = 0.94$
- 30-year LID simulations for NYC, MIA, PHX, and SFO reveal distinct LID runoff partitioning
- The open-source tool supports long-term design and analysis of LID systems

A Coupled Darcy-Richards Framework for Hydrological Modeling of Permeable Pavements, Green Roofs, and Bioretention Systems

Marcus Nóbrega Gomes Jr.^{a,b,*}, Jose Artur Teixeira Brasil^a, Drew Johnson^a, Athanassios T. Papagiannakis^a and Marcio Hofheinz Giacomoni^a

^aThe University of Texas at San Antonio, College of Engineering and Integrated Design, School of Civil Environmental Engineering and Construction Management, One UTSA Circle, San Antonio, 78249, Texas, United States of America

^bThe University of Arizona, Department of Hydrology and Atmospheric Sciences, John W. Harshbarger Building, Tucson, 85719, Arizona, United States of America

ARTICLE INFO


Keywords:

Richards Equation
Low Impact Development (LID)
Infiltration Modeling
Climate Variability
Stormwater Management

ABSTRACT

Urbanization and climate change are accelerating the shift away from pre-development hydrologic regimes, reducing infiltration and baseflow while increasing rapid runoff. While Low Impact Development (LID) strategies such as permeable pavements, green roofs, and bioretention systems offer effective hydrologic mitigation. Existing computational models often oversimplify infiltration processes and lack the capacity for long-term, climate-sensitive simulation. This study introduces a physics-based, open-source modeling framework that couples a one-dimensional mixed-form Richards equation solver with a conceptual surface runoff module and dynamic evaporation and evapotranspiration modeling. The model enables continuous simulation of infiltration-based systems across a range of climate regimes and design configurations. Benchmark against Hydrus-1D showed strong agreement across multiple soil types and boundary conditions, indicating an average RMSE of 0.020 m for pressure head and 0.003 for water content. Model calibration/validation to a monitored field-scale permeable asphalt monitored for 255 days demonstrated high predictive accuracy for calibration (NSE = 0.93, R^2 = 0.94) and validation (NSE = 0.729, R^2 = 0.80). A 30-year continuous simulation for four climatically distinct U.S. cities—New York, Miami, Phoenix, and San Francisco—revealed regional contrasts in runoff retention, evaporation efficiency, and flow duration characteristics. These hydrologic signatures highlighted the potential for groundwater recharge and baseflow support in diverse climates and underscored the importance of maintenance to preserve long-term performance.

*Corresponding author

 marcusnobrega.engcivil@gmail.com (M.N.G. Jr.); arturtbr@gmail.com (J.A.T. Brasil); drew.johnson@utsa.edu (D. Johnson); AT.Papagiannakis@utsa.edu (A.T. Papagiannakis); marcio.giacomoni@utsa.edu (M.H. Giacomoni)

 <https://marcusnobrega-eng.github.io/profile/> (M.N.G. Jr.)

ORCID(s): 0000-0002-8250-8195X (M.N.G. Jr.); 0000-0002-0331-0122 (J.A.T. Brasil); 0000-0002-5550-4922 (D. Johnson); 0000-0002-3047-7112 (A.T. Papagiannakis); 0000-0001-7027-4128 (M.H. Giacomoni)

1. Introduction

Urbanization and climate change are two major drivers affecting the hydrological functioning of cities (Zhou et al., 2019; McGrane, 2016). As urban areas expand, natural land surfaces are replaced by impervious materials such as concrete and asphalt, which significantly reduce infiltration and increase stormwater runoff (Chithra et al., 2015). This shift not only elevates flood risks but also reduces groundwater recharge and alters the timing and volume of flows in receiving water bodies. In parallel, climate change is intensifying rainfall extremes, increasing the frequency and magnitude of storm events in many regions (Westra et al., 2014; Wasko et al., 2021). These combined pressures pose serious challenges for conventional urban drainage systems, which are typically not designed to accommodate such dynamic variability.

In this context, Low Impact Development (LID) practices have emerged as decentralized solutions that promote on-site retention and infiltration of stormwater (Batalini de Macedo et al., 2022b). Common LID techniques—including bioretention systems (Roy-Poirier et al., 2010), permeable pavements (Huang et al., 2016), and green roofs (Li and Babcock Jr, 2014)—aim to restore natural hydrologic processes and reduce the volume and intensity of runoff during storm events. Their performance, however, can vary significantly depending on soil properties, rainfall patterns, and maintenance practices. Understanding how these systems function over time, especially under long-term performance assessments, is essential for ensuring their effectiveness and resilience.

As cities continue to expand and short-term rainfall patterns become more unpredictable, LID practices represent a promising and adaptable solution for building urban resilience (Pugliese et al., 2022). One can design a LID system such that the impact of urbanization can be minimized by the storage capacity and outflow dynamics of a LID system (Olszewski and Davis, 2013). Unlike centralized drainage systems, LIDs are modular and can be implemented at various spatial scales, from individual lots to neighborhood-wide networks (Batalini de Macedo et al., 2022a; McClymont et al., 2020). Their ability to reduce surface runoff (McClymont et al., 2020), enhance groundwater recharge (Dussaillant et al., 2004), and moderate peak flows (Gomes Jr et al., 2023) makes them particularly valuable in managing the compounded effects of urbanization and climate change. Moreover, when properly designed and maintained, LIDs can deliver consistent hydrological benefits over time, even under changing environmental conditions. Incorporating LIDs into long-term urban planning not only supports stormwater control but also aligns with broader sustainability goals by promoting green space, improving microclimates, and enhancing urban livability (Ajirotutu et al., 2024; McClymont et al., 2020).

Despite the recognized importance of LID in urban water management, most tools used to evaluate their hydrologic performance are based on simplified representations of LID-scale hydrological processes, especially the infiltration/exfiltration dynamics. These models typically use empirical or quasi-empirical methods, such as the Soil Conservation Service - Curve Number (SCS-CN) models or Green-Ampt, which do not accurately simulate unsaturated flow dynamics or transitions between wetting and drying conditions (Rossman et al., 2010; Gomes Jr et al., 2023; Skaggs et al., 2012). As a result, key processes such as saturation, drainage, or evaporation may be misrepresented, especially under long-term or climate-sensitive scenarios, making the requirement of Darcy-Richards models necessary to accurately capture the long-term non-linear flow dynamics in these systems.

Physics-based models, particularly those based on complete solutions of the Richards equation, offer a more realistic and detailed representation of water movement in unsaturated porous media. The Richards equation captures the nonlinear behavior of soil water retention and hydraulic conductivity, accounting for both gravity and capillary forces (List and Radu, 2016; Farthing and Ogden, 2017). It is widely used in vadose zone hydrology and has been implemented in software such as Hydrus-1D (Simunek et al., 2005). However, while Hydrus provides a robust platform for simulating unsaturated flow dynamics in porous media, simulating long-term scenarios with coupled rainfall-runoff capabilities is only possible by merging different models, which increases the complexity of application of LID system analysis (Rahman et al., 2025). Users typically need to preprocess forcing data externally and cannot easily simulate LID systems as part of a complete urban drainage framework. This limits its applicability for climate-resilient planning, where integrated and continuous simulation over decades is needed to capture relevant long-term hydrologic signatures expected from LID systems.

Long-term performance analyses using full solutions of the Richards equation are still rare in the literature due to the high computational resources typically required (Pons et al., 2023). Moreover, most tools require external coupling to simulate catchment-scale runoff or evaporation, reducing usability and scalability for integrated urban water planning.

To address these limitations, this study presents a fully coupled, stand-alone modeling framework that integrates a mixed-form, one-dimensional Richards Equation solver with a conceptual rainfall-runoff model. The model simulates event-based and continuous simulations of LID systems, including infiltration, soil moisture redistribution, and surface runoff generation, without the need for external software. It allows for the specification of precipitation and potential evapotranspiration time series which can be directly inserted at LID surface or used to force a catchment-scale hydrological model. In addition, it includes support for layered soil profiles, and can be applied to a wide range of LID designs under different climate conditions when the simplification of 1D modeling is suitable.

The objectives of this work are to: (i) develop and verify the proposed model against a benchmark model (Hydrus-1D) against four cases under different boundary conditions and soils; (ii) validate the model to a monitored permeable pavement site in San Antonio, Texas, to test its real-world applicability; and (iii) simulate the long-term performance by computing hydrologic signatures of bioretention, permeable pavements, and green roofs systems across four contrasting climate regions in the United States over a 30-year climate from 1995 to 2025. A 30-year simulation period captures the effects of seasonal variability, extreme events, and long-term climate trends on LID performance. By applying the model across diverse U.S. climate regions, this study highlights how different rainfall and temperature regimes influence the effectiveness of infiltration-based systems.

The remainder of this paper is organized as follows. Section 2 describes the mathematical formulation and numerical implementation of the model. Three experimental setups for the model are presented in Sec. 3, 4, and 5. Performance metrics evaluated are described in Sec. 6. Sec. 7 presents three applications: (i) model validation against Hydrus-1D; (ii) calibration and testing at a permeable pavement site in Texas; and (iii) long-term LID performance simulation across four U.S. climate zones. Sec. 8 presents the discussions and Section 9 summarizes key findings, limitations, and implications for climate-resilient urban stormwater design.

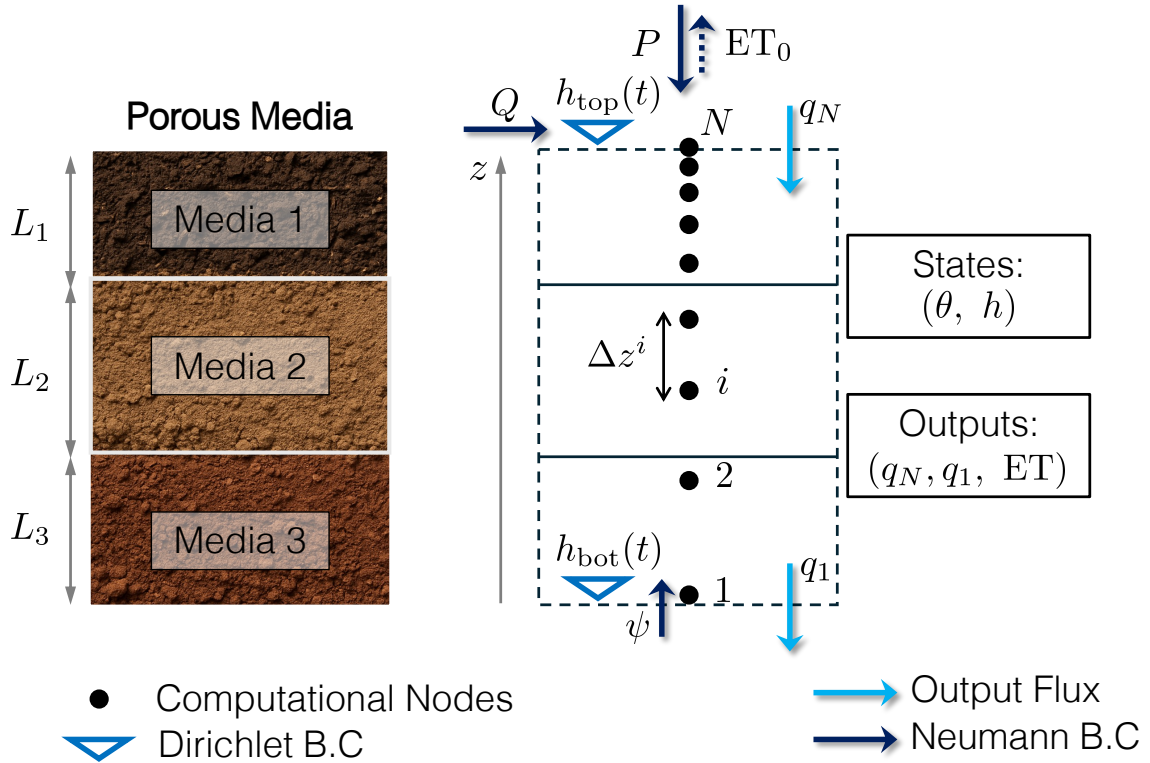


Figure 1: Conceptual schematic of the model domain illustrating real-world stratification of porous media across depths L_1 to L_3 along with the associated numerical mesh discretization. The model supports specification of top Neumann boundary conditions based on upstream discharge (Q), precipitation (P), and reference evapotranspiration (ET_0). Vertical discretization follows a layer-based approach with resolution Δz , which may vary spatially. Both top and bottom boundaries can alternatively be prescribed as Dirichlet conditions. Model outputs include fluxes across domain boundaries and estimates of actual evapotranspiration. Capillary rise flux can be estimated based on a fixed Dirichlet bottom boundary condition (B.C) or by a specified flux ψ . Potential evapotranspiration (blue dashed arrow) equals actual evapotranspiration if water availability conditions are satisfied, as later described.

2. Mathematical Model Development

2.1. 1-D Mixed Form Richards Model Description

The modeling framework developed in this study integrates a one-dimensional, mixed-form Richards solver for variably saturated flow with surface-flux representations for rainfall-runoff generation and evaporation or evapotranspiration. It requires as inputs a combination of meteorological forcing data—precipitation and reference evapotranspiration (ET_0), with the option to prescribe an upstream inflow hydrograph. Layer geometry, boundary condition specifications, and soil or media hydraulic properties must also be specified. The latter are expressed through van Genuchten parameters (α , n , θ_r , θ_s), the saturated hydraulic conductivity (K_s), and the specific storage (S_s). The prognostic states advanced in time are the pressure head $h(z, t)$ and volumetric water content $\theta(z, t)$, from which a range of outputs can be derived. These include boundary fluxes such as infiltration, underdrain or seepage flow, and capillary rise, as well as internal

percolation rates, actual evaporation or evapotranspiration, storage changes, and mass-balance diagnostics. Boundary conditions at the upper surface may be specified as a Neumann flux, with an automatic ponding switch when infiltration capacity is exceeded, or as a Dirichlet pressure head; the lower boundary may be prescribed as free drainage, specified head, or specified flux. The governing Richards equation is discretized in space using a layer-aligned, nonuniform finite-difference mesh, and in time using a fully implicit scheme. The resulting nonlinear system is solved with a Newton–Raphson iteration enhanced by line search, where the residual is formulated from the discrete mass balance, the Jacobian is assembled numerically, and iterations proceed until both head-update and mass-balance tolerances are met. Temporal resolution is dynamically adapted based on iteration performance, subject to user-defined bounds. In the following subsections, we describe the model’s mathematical details.

2.1.1. Governing Equation

Although engineered infiltration media can become saturated during intense storm events, modeling the transition between saturated and unsaturated flow conditions necessitates a shift in the hydraulic framework—typically from saturated models governed by Darcy’s law to those suitable for unsaturated conditions. In the unsaturated zone, flow dynamics are commonly described by the Richards equation (Richards, 1931), which has been applied in various studies and practical implementations (Pons et al., 2023). This equation characterizes the temporal variation of volumetric water content (θ) as a function of the unsaturated hydraulic conductivity (K), the pressure head (h), and a sink term (S) (Richards, 1931), which can be written in the mixed-form as:

$$\frac{\partial \theta(h)}{\partial t} + S_s \frac{\partial h}{\partial t} = \frac{\partial}{\partial z} \left[K(h) \left(\frac{\partial h}{\partial z} + 1 \right) \right] + S(z, t), \quad (1)$$

where h is pressure head [m], $\theta(h)$ is volumetric water content [$\text{m}^3 \text{m}^{-3}$], $K(h)$ is unsaturated hydraulic conductivity [m s^{-1}], S_s is specific storage [m^{-1}], z is vertical coordinate, positive upward taken from the bottom seepage face [m], and $S(z, t)$ is source/sink term [s^{-1}]. By including the specific storage term, the equation handles unsaturated-saturated transitions and prescribes pressure heads as the prognostic state to be solved.

2.1.2. van Genuchten Closed-Form Equations

To numerically solve Eq. 1, however, it is typically necessary to establish a functional relationship between the saturated hydraulic conductivity (K_{sat}) and the volumetric water content (θ). Under unsaturated flow conditions, the soil water retention characteristics can be represented using a closed-form expression, most commonly described by the van Genuchten model (van Genuchten, 1980). This formulation offers the advantage of being both continuous and differentiable, which facilitates its integration into numerical solvers. The model is characterized by two empirical parameters, for which typical estimates and guidance can be found in Simunek et al. (2005). The corresponding closed-form expression for the unsaturated hydraulic conductivity (K) is given as:

$$K(h) = \begin{cases} K_s \frac{\{1 - (\alpha h)^{n-1} [1 + (\alpha h)^n]^{-m}\}}{[1 + (\alpha h)^n]^{m/2}}, & \text{for } h \leq 0 \\ K_s, & \text{Elsewhere,} \end{cases} \quad (2)$$

where $m = 1 - 1/n$ is a shape factor herein assumed, K_s is the saturated hydraulic conductivity of the medium [m s^{-1}], α and n are fitted with experimental data or estimated a priori based on literature.

The water content is estimated as a function of media constitutive relationship parameters as (van Genuchten, 1980):

$$\theta(h) = \begin{cases} \theta_r + (\theta_s - \theta_r) [1 + (\alpha|h|)^n]^{-m}, & h < 0 \\ \theta_s, & h \geq 0 \end{cases} \quad (3)$$

where θ_r denotes the residual water content [–], θ_s is the saturated water content [–], α represents the inverse air-entry pressure [m^{-1}], and n is the pore-size distribution parameter [–].

The flow rates in each cell edges is estimated by the following finite-difference approximations (Simunek et al., 2005), assuming the values of hydraulic conductivity for half-nodes estimated by arithmetic averages (Farthing and Ogden, 2017):

$$q_1^{j+1} = -K_{1+1/2}^{j+1} \left(\frac{h_2^{j+1} - h_1^{j+1}}{\Delta z_i} + 1 \right) \quad (4a)$$

$$q_i^{j+1} = \frac{-K_{i+1/2}^{j+1} \left(\frac{h_{i+1}^{j+1} - h_i^{j+1}}{\Delta z_i} + 1 \right) \Delta z_{i-1} - K_{i-1/2}^{j+1} \left(\frac{h_i^{j+1} - h_{i-1}^{j+1}}{\Delta z_{i-1}} + 1 \right) \Delta z_i}{\Delta z_{i-1} + \Delta z_i} \quad (4b)$$

$$q_N^{j+1} = -K_{N-1/2}^{j+1} \left(\frac{h_N^{j+1} - h_{N-1}^{j+1}}{\Delta z_{N-1}} + 1 \right) - \frac{\Delta z_{N-1}}{2} \left(\frac{\theta_N^{j+1} - \theta_N^j}{\Delta t} + S_N^j \right), \quad (4c)$$

where q_i^{j+1} denotes the vertical water flux at node i and time step $j + 1$ [L T^{-1}]. The pressure head at node i and time step $j + 1$ is given by h_i^{j+1} [L], and Δz represents the vertical spacing between adjacent nodes [L]. The number of nodes is defined by N . The hydraulic conductivity at the midpoint between nodes i and $i \pm 1$, evaluated at time step $j + 1$, is denoted by $K_{i\pm 1/2}^{j+1}$ [L T^{-1}]. The volumetric water content at node i at time steps j and $j + 1$ are represented by θ_i^j and θ_i^{j+1} , respectively [–]. S_i^j denotes the volumetric source or sink term at node i and time step j [T^{-1}].

A set of different boundary condition types, including Neumann (specified flux), Dirichlet (specified head), and free-flow, is available in the model and is described in detail in the supporting information. An adaptive top boundary condition adjustment is done when ponding occurs in cases where top flux as Neumann boundary condition is specified (Simunek et al., 2005). Additionally, modeling orifices and spillways is also permitted and further detailed in the model manual for reference.

2.1.3. Numerical Discretization

We solve the dynamic flow problem in a partially saturated 1-D rigid medium by computing the residual of Eq. (1). In a k -th Newton-Raphson iteration, the residual can be defined as:

$$F_i^{k+1} = \frac{\theta_i^{k+1} - \theta_i^k}{\Delta t} + S_s \cdot \frac{h_i^{k+1} - h_i^k}{\Delta t} + \frac{q_{i+1/2}^{k+1} - q_{i-1/2}^{k+1}}{\Delta z_i} - S_i^{k+1}, \quad (5)$$

where F_i^{k+1} is the residual at node i at iteration k computed as the difference between left and right hand-side of a discrete form of Eq. (1).

By linearizing the problem computing the numerical Jacobian $\mathbf{J} := \frac{\partial \mathbf{F}}{\partial \mathbf{h}}$, one can solve a series of linear systems of equations presented in Eq. (6) and update the node heads in Eq. (7) for the Newton-Raphson algorithm such that:

$$\mathbf{J}^k \cdot \Delta \mathbf{h}^k = -\mathbf{F}^k \quad (6)$$

$$\mathbf{h}^{k+1} = \mathbf{h}^k + \lambda \cdot \Delta \mathbf{h}^k, \quad (7)$$

where $\mathbf{J}^k \in \mathbb{R}^{n \times n}$ is the Jacobian matrix at iteration k [m^{-1}], $\Delta \mathbf{h}^k \in \mathbb{R}^n$ is the Newton update direction [m], and λ is a line search step size with $0 < \lambda \leq 1$. Details on the line-search approach can be found in the model manual.

Convergence of the iterative procedure may be assumed when the 2-norm of the Newton-Raphson update, $\|\Delta h\|_2$, falls below a prescribed tolerance, $\delta \approx 10^{-6}$, and/or when the mass balance error over a time step does not exceed a threshold m_{tol} , typically on the order of 10^{-3} to 10^{-6} .

2.1.4. Adaptive Time Stepping

Time step size Δt is adaptively updated after each successful (i.e., convergence criteria of mass balance and pressure head deviation smaller than tolerance) iteration based on the number of iterations required for convergence, n_{iter} (Simunek et al., 2005; Farthing and Ogden, 2017):

$$\Delta t_{\text{new}} = \begin{cases} \min(\Delta t \cdot \beta_{\text{up}}, \Delta t_{\text{max}}) & \text{if } n_{\text{iter}} \leq n_{\text{up}} \\ \max(\Delta t \cdot \beta_{\text{down}}, \Delta t_{\text{min}}) & \text{if } n_{\text{iter}} \geq n_{\text{down}} \\ \Delta t & \text{otherwise,} \end{cases} \quad (8)$$

where β_{up} and β_{down} are multiplicative factors used to increase or decrease the time step, respectively. The thresholds n_{up} and n_{down} define iteration limits for time step adjustment. Time step bounds Δt_{min} and Δt_{max} are user-defined and are problem-specific.

2.1.5. Evapotranspiration/Evaporation Modeling

The Hargreaves method is an empirical approach used to estimate reference evapotranspiration (ET_0) based primarily on temperature data and extraterrestrial solar radiation (Hargreaves and Samani, 1982). It is particularly suitable for regions where only limited meteorological data are available, making it a practical alternative to more data-intensive methods such as the Penman-Monteith equation. The method assumes that temperature differences provide a reliable proxy for solar radiation and atmospheric demand, based on the rationale that higher diurnal temperature ranges typically reflect greater evapotranspirative potential. Reference evapotranspiration using the Hargreaves method is calculated as (Hargreaves and Samani, 1982):

$$ET_0 = 0.0023 \cdot (T_{\text{mean}} + 17.8) \cdot (T_{\text{max}} - T_{\text{min}})^{0.5} \cdot R_a, \quad (9)$$

where ET_0 is the reference evapotranspiration (mm/day), T_{mean} is the average daily air temperature ($^{\circ}\text{C}$), T_{max} and T_{min} are the daily maximum and minimum temperatures ($^{\circ}\text{C}$), respectively, and R_a is the extraterrestrial radiation ($\text{MJ}/\text{m}^2/\text{day}$). The extraterrestrial radiation R_a depends on latitude and time of year and can be computed from astronomical formulas (Hargreaves and Allen, 2003).

To account for the limitations imposed by water content availability on upward water movement, the model incorporates the Feddes reduction function (Feddes et al., 1976). This function modifies the potential surface vertical flux based on the surface pressure head h , yielding an actual flux that reflects the physical limitations of the media's hydraulic properties. The effective evaporation flux is given by (Simunek et al., 2005):

$$q_{\text{ET}} = \alpha(h) \cdot ET_0, \quad (10)$$

where $\alpha(h) \in [0, 1]$ is the evaporation reduction coefficient. The function $\alpha(h)$ is defined as a continuous, piecewise-linear function dependent on two user-specified pressure head thresholds: $h_{\text{lim, upper}}$, the wet-limit above which full evaporation occurs, and $h_{\text{lim, lower}}$, the dry-limit below which evaporation ceases. The mathematical expression is given by (Feddes et al., 1976):

$$\alpha(h) = \begin{cases} 1, & h \geq h_{\text{lim, upper}} \\ \frac{h - h_{\text{lim, lower}}}{h_{\text{lim, upper}} - h_{\text{lim, lower}}}, & h_{\text{lim, lower}} < h < h_{\text{lim, upper}} \\ 0, & h \leq h_{\text{lim, lower}} \end{cases} \quad (11)$$

For non-vegetated systems such as permeable pavements, observed evaporation is approximately 30% of gross pan evaporation (Huang et al., 2016; Li et al., 2014; Liu et al., 2018). A daily bias (δ) between pan evaporation and estimated reference evapotranspiration can be incorporated through regression analysis (Gomes Jr et al., 2021). From the best of our knowledge, no scientifically validated expression for evaporation in permeable pavements is available in the literature. We hence propose an empirical expression for the potential evaporation from permeable pavements (E_0), which is then expressed as:

$$E_0 = \gamma (ET_0 + \delta), \quad (12)$$

where E_0 is the potential evaporation from permeable pavements [mm/day], γ is the evaporation ratio (assumed to be 0.3), and δ is the daily bias (assumed to be 2 mm/day) (Gomes Jr et al., 2021). Equation (10) remains valid by replacing ET_0 with E_0 for permeable pavement conditions.

2.2. Catchment-scale Hydrological Modeling

The catchment hydrologic model uses a lumped conceptual approach where the watershed is treated as a non-linear reservoir with an average time-varying flow depth h^w (Rossman et al., 2010). Water is conveyed through a simplified rectangular channel that includes a weir with threshold depth h_0^w as a proxy for the catchment initial abstractions. Outflow only occurs if $h^w > h_0^w$. The flow dynamics are governed by the kinematic wave approximation of the shallow water equations, where the energy slope is approximated by the bed slope s_0 . The resulting discharge $q^w(t)$ is estimated using Manning's equation:

$$q^w(t) = \frac{1}{n^w} w^w \max(h^w(t) - h_0^w, 0)^{5/3} s_0^{1/2}, \quad (13)$$

where n^w is the Manning roughness coefficient and w^w is the average width of the watershed.

The mass balance in the watershed reservoir can be represented by a partial differential equation that describes the time evolution of water depth $h^w(t)$ based on the difference between effective precipitation input and outflow discharge. Assuming a spatially lumped system, the governing equation is:

$$\frac{\partial h^w(t)}{\partial t} = \frac{1}{a^w} (p_{ef}(t) - q^w(t)),$$

where a^w is the watershed area, $p_{ef}(t)$ is the effective precipitation rate (e.g., estimated by the SCS-CN method with adjustments for continuous simulation modeling (Rossman et al., 2010)), and $q^w(t)$ is the outflow discharge as governed by Manning's equation. This continuous-time formulation allows for dynamic simulation of runoff generation and routing within the catchment, supporting both input-driven hydrographs and physically-based rainfall-runoff processes, and is numerically solved with a forward Euler scheme. Although the model solves the non-linear reservoir dynamics of SWMM (Rossman et al., 2010), users can input inflow hydrographs from different models or only force the 1D media with net rainfall timeseries.

3. Model Verification - Benchmarking Against Hydrus-1D

Four case studies were conducted to assess the model's performance under various soil types, moisture conditions, and boundary constraints. Each simulation was evaluated against Hydrus-1D outputs for both pressure head and volumetric moisture content. Example 1 involved constant infiltration into a dry sandy soil, representing a highly conductive medium. The top boundary condition was specified as a fixed pressure (Dirichlet), allowing for a sharp wetting front without surface ponding. Example 2 explored infiltration into a dry clay loam soil with lower saturated conductivity and higher initial suction. This case featured the same Dirichlet top boundary

condition but resulted in a more diffuse wetting front due to the finer soil texture. Example 3 simulated a capillary rise from a shallow water table into a dry vadose zone. Both top and bottom boundaries were defined using Dirichlet conditions, with saturation imposed at the bottom and a dry condition at the surface. Example 4 replicated the sandy soil scenario from Example 1 but replaced the top boundary condition with a constant flux (Neumann) to simulate uniform rainfall infiltration at a rate of 1 m/day. Details of input data used in each of the cases are available in SI.

4. Model Calibration / Validation - Permeable Asphalt in San Antonio, Texas

The study was conducted at a fully instrumented field site located within a 0.8 km² public natural park, which serves both as a high-traffic parking area and a habitat for local wildlife. Among the four permeable pavement (PP) types constructed at the site, this study focuses exclusively on the Permeable Asphalt (PA) section. All pavement cells, including the PA, share identical surface dimensions of 10.7 m × 19.8 m, corresponding to eight standard parking stalls.

The PA pavement consists of an asphalt mix designed to permit surface infiltration, placed over a common structural base shared by all permeable pavement types. The underlying structure includes a 10.2 cm layer of ASTM No. 8 washed gravel over a 20.3 cm layer of ASTM #2 washed crushed stone, resulting in a total base/subbase thickness of 30.5 cm. This configuration was designed to provide temporary water storage and support traffic loads. Based on a design porosity of 0.4, the storage capacity was estimated at 24.4 m³, which is sufficient to accommodate a 50-year design storm producing 304.5 mm of rainfall over the approximately 200 m² surface area.

The entire system is hydraulically isolated to ensure that all water entering the pavement surface originates from direct rainfall. Surrounding curbs, geotextiles, and surface grading prevent any lateral inflow or outflow. Infiltrated water is collected via a 15.24 cm perforated underdrain pipe installed beneath the aggregate layers. The pipe has a perforation pattern engineered to ensure that the total open area exceeds the pipe's cross-sectional area, thereby avoiding hydraulic restrictions and preserving efficient drainage performance. This pipe, under saturated conditions, can convey a discharge rate of approximately 500 mm/h, which, under current typical rainfall conditions, has a very low chance of occurrence. Therefore, a free-flow boundary condition is assumed at the permeable pavement bottom seepage face.

Monitoring of the PA cell includes continuous measurement of rainfall and underdrain outflow. Rainfall is recorded using two 6-inch Texas Electronics TR525I tipping bucket rain gauges. Outflow from the PA pavement is monitored with an ISCO Bubbler flowmeter and an ISCO 6712 autosampler. Water levels measured in the underdrain are converted to flow rates using a calibration curve for a 6-inch V-Notch Thel-Mar weir. These measurements support detailed hydrologic performance analysis of the permeable asphalt system under real-world rainfall conditions.

Model calibration was performed by maximizing the Nash-Sutcliffe-Efficiency (NSE) (Nash and Sutcliffe, 1970) with an automatic calibration algorithm solver using genetic algorithms. From the 262-day monitoring period (10/04/2023 to 06/02/2024), the time window from 12/21/2023 to 01/27/2024 was selected for model calibration. This 37-day period includes four distinct rainfall-runoff events, providing sufficient hydrologic variability to constrain key model parameters. The relatively short duration facilitates computational efficiency during the automatic calibration process, which requires multiple model evaluations. By concentrating several events within a

compact timeframe, this period offers a favorable trade-off between hydrologic representativeness and the practical demands of iterative optimization.

The calibration targets key media properties, including the van Genuchten parameters α (1/m) and n (-), residual and saturated water contents (θ_r , θ_s), saturated hydraulic conductivity K_s (m/s), and specific storage S_s (1/m). These parameters were estimated independently for each soil layer, resulting in a concatenated parameter vector. Parameter bounds were defined to ensure physical plausibility: $\alpha \in [3, 15] \text{ m}^{-1}$, $n \in [1.25, 3.0]$, $\theta_r = 0.005$, $\theta_s \in [0.20, 0.50]$, $S_s = 1 \times 10^{-5} \text{ m}^{-1}$, and $K_s \in [1 \times 10^{-5}, 1 \times 10^{-2}] \text{ m/s}$. The residual water content and specific storage were held constant in this setup.

The selection of parameter bounds for calibration was informed by the physical characteristics of layered permeable pavement systems and supported by values reported in the literature for porous asphalt, gravel bases, and aggregate subgrades (Huang et al., 2016; Gomes Jr et al., 2021; Simunek et al., 2005). The van Genuchten parameter $\alpha \in [3, 15] \text{ m}^{-1}$ was chosen to reflect the rapid air-entry behavior typical of coarse granular media, while $n \in [1.25, 3.0]$ captures a range of pore-size distributions expected across surface and subbase layers. The saturated water content $\theta_s \in [0.20, 0.50]$ spans typical porosities of porous asphalt (lower end) to highly voided stone reservoirs (upper end), whereas a fixed residual water content $\theta_r = 0.005$ was assumed given the limited moisture retention of clean, non-cohesive aggregates. The saturated hydraulic conductivity $K_s \in [10^{-5}, 10^{-2}] \text{ m/s}$ accommodates the transition from partially clogged surface layers to highly permeable stone storage zones. Specific storage was held constant at $S_s = 1 \times 10^{-5} \text{ m}^{-1}$, given its limited influence under unsaturated conditions but utility in maintaining numerical stability near saturation. These parameter bounds balance physical plausibility with calibration flexibility, ensuring that the hydraulic behavior of the multilayered pavement system is accurately represented while preserving solver robustness.

Calibration was performed using a genetic algorithm (GA), which iteratively minimizes the objective function by evolving a population of parameter sets. The objective function is based on the Nash–Sutcliffe Efficiency (NSE) between the simulated and observed outflow discharge, with higher NSE values indicating better model performance. A penalty is applied when the solver fails or the observed discharge is constant. The GA was configured in MATLAB with a population size of 40, a maximum of 10 generations, and a fitness tracking function to monitor convergence behavior. At each iteration, the solver is called with a candidate parameter set, and the resulting fluxes at the bottom node are compared to observed discharge data. Model performance is evaluated after a warm-up period of approximately 3 days to eliminate initialization bias from presumed initial head conditions.

5. Model Application: Estimating the Long-Term Hydrological Behavior of LID structures under different climates

To ensure a hydrologically consistent and technically sound comparison, all LID systems were simulated using a fixed impervious drainage area of 500 m^2 , representing a typical catchment area for retrofitting LID systems. The model is forced with daily rainfall, and with maximum and minimum temperature from 01/01/1995 to 01/01/2025, climate with the objective of capturing long-term variability for LID. Forcing data is linearly interpolated when time steps are smaller than the source data resolution. The green roof and permeable pavement systems were assumed to cover the entire contributing area (1:1 ratio), representing rooftop and surface-integrated designs,

Table 1

Design specifications and van Genuchten parameters for the simulated LID systems. All systems were assigned a contributing area of 500 m². The bioretention cell was sized at 50 m² (footprint ratio 0.10), while the permeable pavement and green roof covered the full catchment area (footprint ratio 1.00). All bottom boundaries were modeled as free drainage. Atmospheric fluxes were modeled as evapotranspiration for bioretention and green roofs, and as evaporation for permeable pavement. Hydraulic parameters for permeable pavement were obtained through calibration; others were sourced from the literature.

LID Type	Layer	Depth (m)	α (1/m)	n (-)	θ_r	θ_s	K_s (cm/min)	S_s (1/m)
Bioretention Cell	Filter media (sandy loam)	0.6	12.4	2.3	0.057	0.410	0.24	1.00E-05
	Gravel bed	0.3	3.5	1.8	0.005	0.450	5.25	1.00E-05
Permeable Pavement	Wear layer	0.025	3.5	1.8	0.005	0.458	120.00	1.00E-05
	Crushed stone base	0.1	6.1	2.5	0.005	0.211	39.00	1.00E-04
	Stone storage (subbase)	0.2	6.0	1.6	0.005	0.204	37.80	1.00E-04
Green Roof	Filter media (sandy loam)	0.1	12.4	2.3	0.057	0.410	0.24	1.00E-05

respectively. In contrast, the bioretention system was sized at 10% of the contributing area (50 m²) (Gomes Jr et al., 2023; Dussaillant et al., 2004), consistent with urban design guidelines.

For the bioretention cases, an upstream contributing area is assumed as a representative urban catchment with dimensions of 50 meters in length and 10 meters in width, totaling an area of 500 m², hence with a compactness coefficient of approximately 1.5. The land use distribution assumed consists of 80% impervious surfaces and 20% pervious surfaces, characterized by curve numbers (CN) of 95 and 65, respectively. The resulting composite curve number was computed as 89 and used to estimate the initial abstract ($h_0 = 6$ mm), following standard SCS methodology. Surface roughness was set using Manning's coefficient $n = 0.02 \text{ s} \cdot \text{m}^{-1/3}$, typical for mixed pavement and lawn areas, and the average slope was assumed to be 1.5% ($S = 0.015$). These parameters were used in the SCS-based hydrologic model to compute runoff hydrographs in a continuous simulation fashion directed to a bioretention system for further hydraulic analysis. The catchment saturated hydraulic conductivity was set to $K_s = 10$ mm/h, representing moderately permeable urban soils such as compacted loam, and was used to compute the empty time (Rossman et al., 2010) for groundwater replenishing. A recovery rate of $K_r = 2$ mm/h (20% of K_s) was assumed to account for catchment-scale infiltration recovery (Rossman et al., 2010).

Each LID was assigned representative physical and hydraulic properties based on results from this paper or from the literature (Simunek et al., 2005) as described in Tab. 1. Performance metrics—including total runoff volume reduction, peak flow attenuation, runoff coefficient, evaporation coefficient, and infiltration volume—were computed and compared within each LID type.

Vertical spatial discretization for the Richards solver was performed using 27 non-uniformly distributed nodes, with higher density near the land surface to meet mesh refinement criteria (see SI for details) (Simunek et al., 2005). Iteration convergence was set to 10^{-6} and mass balance iteration tolerance to 10^{-5} m. Upper and lower time-step multiplicative factors following Eq. (8) were assumed as 2 and 0.5, respectively. Maximum and minimum time-steps were adopted as 86400 and 0.01 seconds, respectively.

Table 2

Summary of performance metrics used to evaluate model performance, including error-based, correlation-based, and volume-based indicators. In the KGE metric, r is the linear correlation between observed and simulated values, $\alpha = \sigma_{\text{sim}}/\sigma_{\text{obs}}$ is the ratio of simulated to observed standard deviation (representing relative variability), and $\beta = \mu_{\text{sim}}/\mu_{\text{obs}}$ is the ratio of simulated to observed mean discharge (representing bias in magnitude). The evaporation coefficient (EC) is the ratio of total evaporation to total precipitation. The term n_{obs} denotes the number of observed data points used in the evaluation.

Metric	Formula	Range
NSE (Nash–Sutcliffe Efficiency)	$\text{NSE} = 1 - \frac{\sum (Q_{\text{obs}} - Q_{\text{sim}})^2}{\sum (Q_{\text{obs}} - \bar{Q}_{\text{obs}})^2}$	$(-\infty, 1]$
RMSE (Root Mean Square Error)	$\text{RMSE} = \sqrt{\frac{1}{n_{\text{obs}}} \sum (Q_{\text{obs}} - Q_{\text{sim}})^2}$	$[0, \infty)$
PBIAS (Percent Bias)	$\text{PBIAS} = 100 \cdot \frac{\sum (Q_{\text{sim}} - Q_{\text{obs}})}{\sum Q_{\text{obs}}}$	$(-\infty, \infty)$
KGE (Kling–Gupta Efficiency)	$\text{KGE} = 1 - \sqrt{(r - 1)^2 + (\alpha - 1)^2 + (\beta - 1)^2}$	$(-\infty, 1]$
R^2 (Coefficient of Determination)	$R^2 = \left(\frac{\sum (Q_{\text{sim}} - \bar{Q}_{\text{sim}})(Q_{\text{obs}} - \bar{Q}_{\text{obs}})}{\sqrt{\sum (Q_{\text{sim}} - \bar{Q}_{\text{sim}})^2} \sqrt{\sum (Q_{\text{obs}} - \bar{Q}_{\text{obs}})^2}} \right)^2$	$[0, 1]$
RC (Runoff Coefficient)	$\text{RC} = \frac{\sum Q_{\text{sim}} \cdot \Delta t}{\sum P \cdot \Delta t} = \frac{Q_{\text{sim, total}}}{P_{\text{total}}}$	$[0, 1]$
EC (Evaporation Coefficient)	$\text{EC} = \frac{E_{\text{total}}}{P_{\text{total}}}$	$[0, 1]$

To evaluate the hydrological performance of different Low Impact Development (LID) strategies, we simulate their behavior under distinct climatic conditions using representative cities listed in Fig. 2. These cities were selected to capture a wide range of hydroclimatic variability across the United States, including differences in precipitation regimes, evapotranspiration demand, temperature seasonality, and storm intensity. This selection enables a robust assessment of LID system performance under diverse environmental stresses, such as arid heat, tropical rainfall, winter snow, and seasonal drought. Snowpack and snowmelt processes are not considered in the current version of this model, and all precipitation is assumed as rainfall. This approximation is valid for the cities studied, especially because the minimum temperature duration curves presented in Fig. 2 indicate a small part of the time under freezing conditions. Lateral exfiltration is neglected in all cases, and bottom seepage flow under free-flow conditions is assumed as Q .

6. Performance Indicators

To evaluate the performance of the hydrological model in simulating discharge, several statistical metrics were employed. These metrics provide insight into different aspects of model behavior, such as accuracy, bias, variability, and correlation with observed data. Table 2 summarizes the formulas, interpretation ranges, and descriptions of each metric.

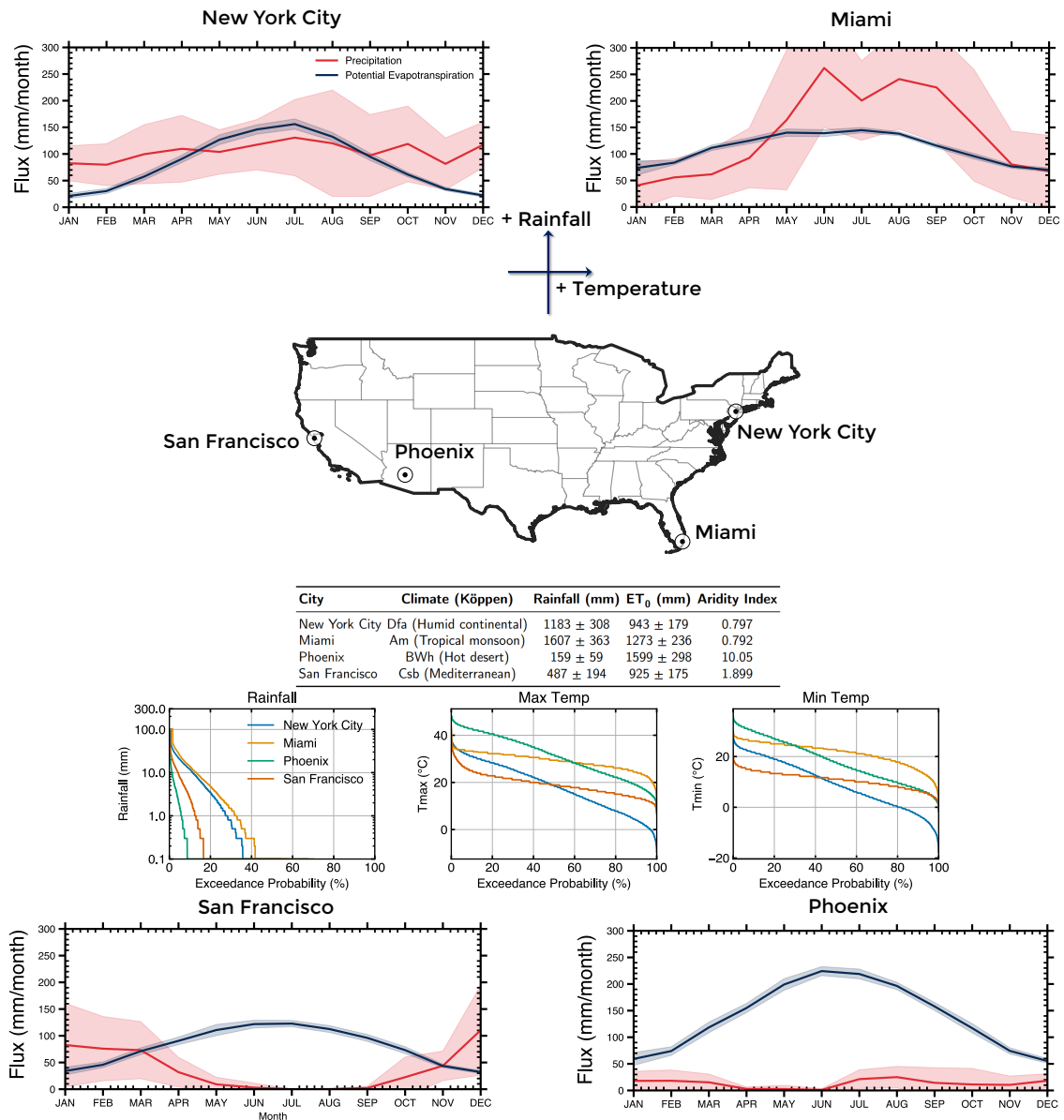


Figure 2: Climatic characterization of four U.S. cities across distinct Köppen zones. Top and bottom panels show monthly precipitation and potential evapotranspiration (ET_0 , Hargreaves method) with multi-year means and ± 1 standard deviation (1995–2025). Rainfall exhibits high interannual variability, while ET_0 is comparatively stable. Duration curves (1995–2015) present daily exceedance probabilities for precipitation, maximum, and minimum temperature. The central table summarizes average annual rainfall, ET_0 , and aridity indices. Data from Meteostat (<https://meteostat.net/en/>).

7. Results

7.1. Model Benchmarking

Across all four test cases, the model demonstrated strong agreement with Hydrus-1D results in simulating pressure head and moisture content dynamics (see Figs. S1 - S4 in the SI for time-varying dynamics of RMSE and Fig. 3). In Example 1, a sharp wetting front propagated rapidly

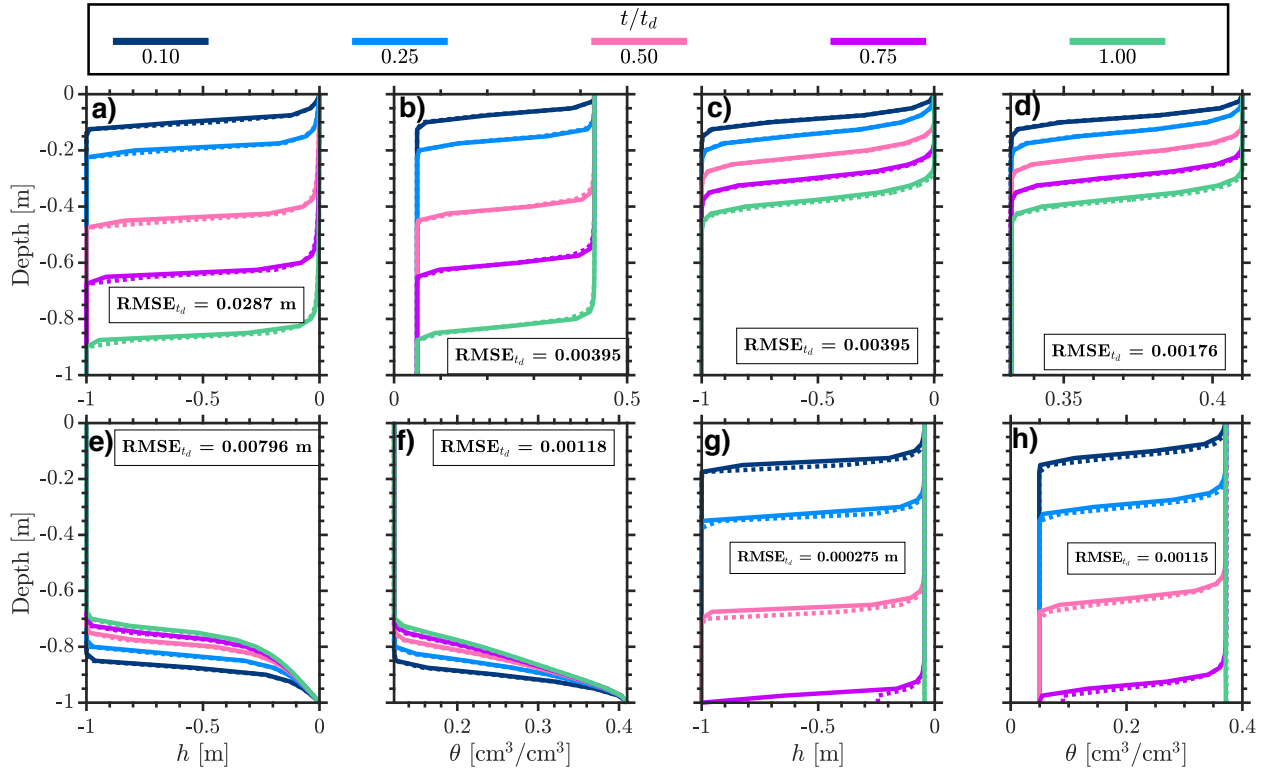


Figure 3: Comparison between simulated (dotted lines) and Hydrus-1D benchmark (solid lines) profiles of pressure head h and volumetric water content θ for the four verification cases described in Section 3. Panels (a)–(d) correspond to: (a–b) Example 1 — constant pressure head infiltration into a dry sandy soil over $t_d = 1$ h; (c–d) Example 2 — constant pressure head infiltration into a dry clay loam over $t_d = 10$ h. Panels (e)–(h) correspond to: (e–f) Example 3 — capillary rise from a shallow water table into a dry profile over $t_d = 10$ h; (g–h) Example 4 — constant-flux infiltration into a sandy soil over $t_d = 1$ h. Colors indicate the normalized simulation time $t/t_d = 0.10, 0.25, 0.50, 0.75$, and 1.00 as shown in the top legend. Root Mean Square Error (RMSE) values quantify agreement between the model and Hydrus-1D outputs for each profile. Depth is positive downward from the surface, with free-drainage lower boundaries unless otherwise specified.

through the sandy soil. The root mean square error (RMSE) values for both pressure head and volumetric moisture content remained low (< 0.05) throughout the simulation, confirming accurate performance.

Example 2 showed a slower, more gradual infiltration process due to the finer clay loam texture. The model effectively captured the delayed onset of infiltration and gradual wetting front progression. RMSE values remained consistently low ($\text{RMSE} \approx 0.02$), and profile comparisons revealed excellent alignment with Hydrus-1D, particularly during mid-simulation times. In Example 3, the model reproduced the upward movement of water through capillary rise with good accuracy. The RMSE values indicated high fidelity ($\text{RMSE} < 0.01$) to the Hydrus-1D solution, and the model captured both the pressure and moisture gradients throughout the soil column.

Example 4 validated the model's performance under a constant rainfall input using a Neumann top boundary. The results closely matched Hydrus-1D ($\text{RMSE} < 0.05$), with only minor deviations

near the surface at later times, likely due to differences in surface boundary condition implementation.

Overall, the model produced similar estimates of infiltration and capillary dynamics across varied soil types and boundary configurations compared to Hydrus-1D. Differences are primarily observed due to convergence criteria and mass-balance tolerance thresholds, which in our case we considered a tolerance of 10^{-6} m per iteration.

7.2. Model Calibration / Validation

Modeling results of the calibration phase applied for the permeable pavement in San Antonio, Texas, are presented in Fig. 4 (a)-(d), resulting in $NSE = 0.937$ and $RMSE = 0.31$ mm/h. The model presented accurate results for high flows, as expected by the usage of NSE as a calibration metric. Results are also accurate for parts of the low-flow events; however, significant differences occurred in the simulated and observed runoff coefficients of 0.93 and 0.68, respectively. Validation results are presented in Fig. 4 (e)-(h) indicate $NSE = 0.729$ and $RMSE = 0.28$ mm/h. A relatively lower performance, although still acceptable, was observed, with the model accurately predicting most of the peak flows but with phases of under- and over-estimations for low to mid flows, as shown in Fig. 4. Similar performance results were found in Brunetti et al. (2016) using Hydrus-1D.

7.3. Model Application

The duration curves in Fig. 2 highlight distinct climate forcing patterns across New York City, Miami, Phoenix, and San Francisco from 1995 to 2025. Miami shows the highest rainfall intensities, while Phoenix and San Francisco experience fewer heavy rainfall events. Rain-day exceedance probabilities (rainfall ≤ 0.1 mm) vary widely, with values of approximately 9% in Phoenix, 18% in San Francisco, 35% in New York City, and 42% in Miami. Phoenix also exhibits the highest maximum and minimum temperatures, reflecting intense heat and limited nocturnal cooling. Miami shows warm but stable conditions, while San Francisco remains mild year-round. New York displays a broad temperature range due to strong seasonality. These curves underscore regional differences in climate exposure relevant to urban resilience and ultimately play a role in the partitioning of rainfall into runoff and evaporation/evapotranspiration.

The runoff and evaporation coefficients computed for each LID configuration across the four studied cities are presented in Table 3. These coefficients represent the proportion of total precipitation that leaves the system either through sub-surface discharge (Q/P) or is lost via evaporation or evapotranspiration (E/P), offering a high-level summary of the long-term water balance. The results demonstrate strong climatic control over LID hydrologic performance. In arid climates such as Phoenix, evaporation dominates, accounting for up to 74% of precipitation in the bioretention cell, while only 26% is discharged. In contrast, cities with humid climates, such as Miami and New York City, show higher runoff coefficients ranging from 67–75% and lower evaporation proportions, reflecting limited atmospheric demand relative to water availability and hence can be classified as energy-limited areas. San Francisco, with its Mediterranean climate, exhibited the highest runoff ratios (up to 86%) and the lowest evaporation contribution, highlighting its seasonal rainfall concentration and cooler temperatures. Although a relatively high aridity index is observed in San Francisco, most of its rainfall volumes occur in the winter seasons, generating an energy-limited condition, which favors the runoff generation. While all LID types respond to climatic forcing, bioretention systems tend to favor infiltration and evapotranspiration more than permeable pavements and green roofs in arid settings. This is likely due to their deeper profiles,

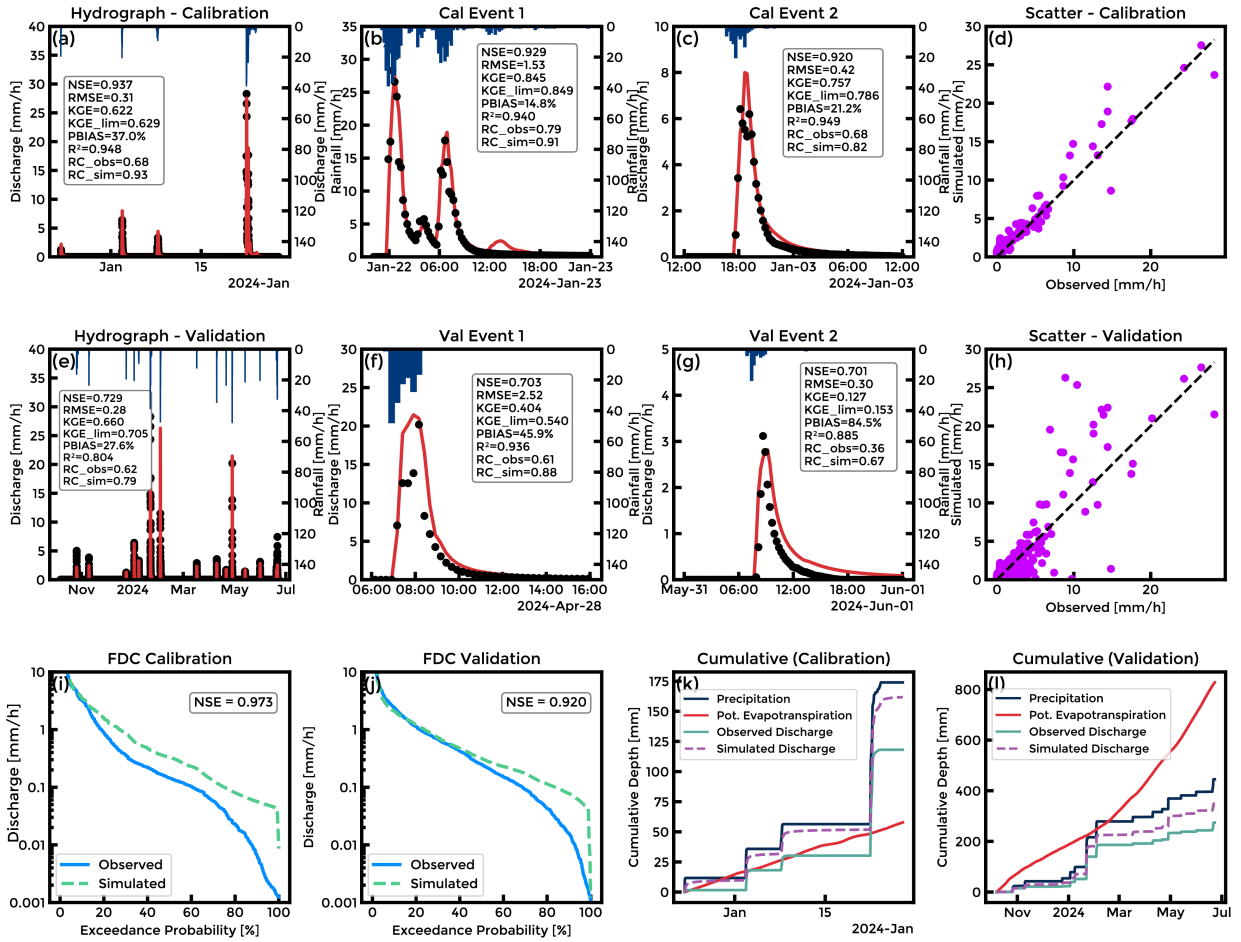


Figure 4: Overview of hydrological model performance during calibration and validation. Top and middle rows (a–h) show time series plots for discharge and rainfall, including overall hydrographs, selected rainfall-runoff events, and parity plots comparing observed and simulated discharge. Performance metrics such as NSE, RMSE, KGE, PBIAS, R^2 , and runoff coefficients (RC) are displayed for each case. The bottom row (i–l) includes flow duration curves (FDCs) and cumulative water balance plots for both periods. FDC plots (i–j) illustrate the distribution of flow exceedance probabilities, while cumulative plots (k–l) show aggregated rainfall, potential evapotranspiration, and observed and simulated discharge over time.

vegetated surfaces, and footprint area of 10% of the drainage area, which results in sustained inflow discharges over longer periods.

8. Discussion

8.1. Model Performance

The numerical experiments comparing the developed model with Hydrus-1D demonstrate good accuracy with low model deviations under various boundary conditions and different media characteristics. Differences are primarily derived from solver convergence criteria and type used. Hydrus-1D uses a modified Picard iteration method, whereas we approach the solution with a Newton-Raphson algorithm.

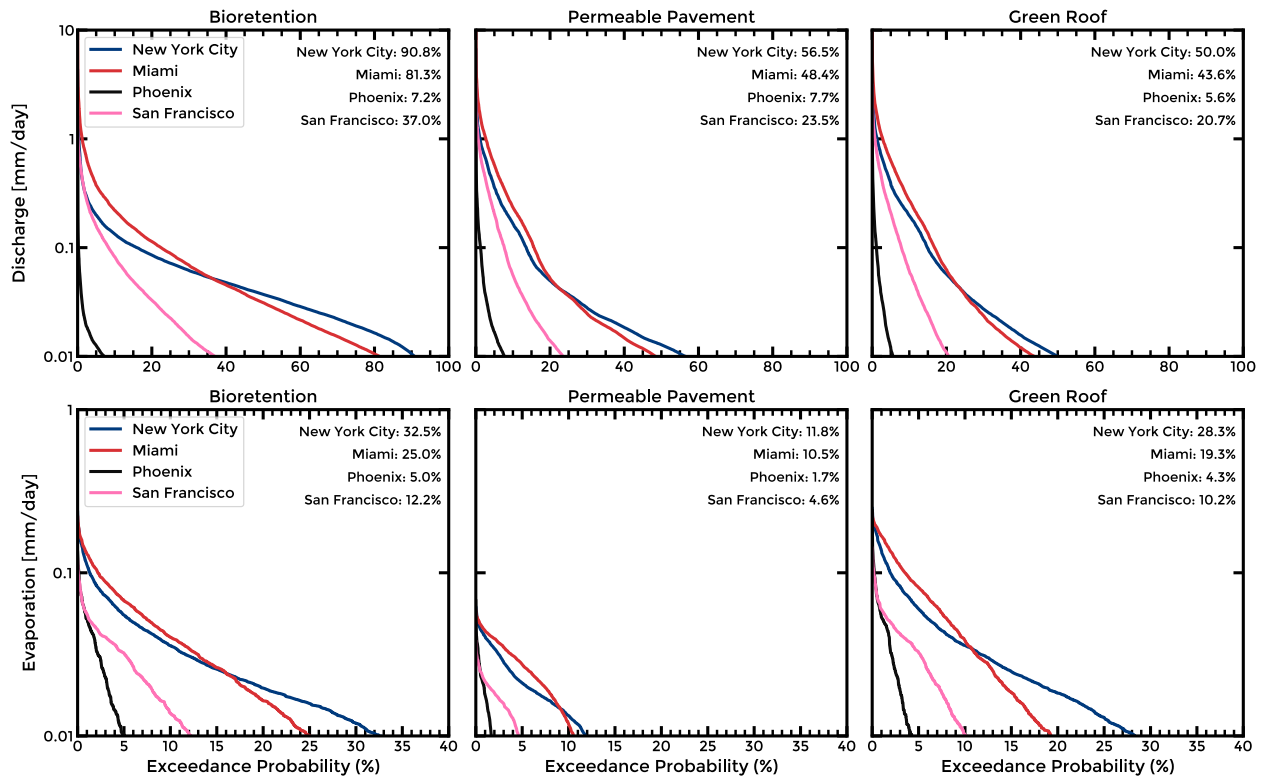


Figure 5: Flow and evaporation/evapotranspiration duration of each LID type per city sampled at daily time-steps. Annotations in each plot indicate the exceedance probability in which the fluxes are not greater than 0.01 mm/day. Only vertical fluxes when rainfall is not occurring are considered in this analysis.

Table 3

Partitioning of long-term water balance into runoff (Q/P) and evaporation (E/P) fractions for three types of LID practices across four U.S. cities. Values represent the percentage of total precipitation (P) that leaves the system as sub-surface discharge (Q) or is lost through evaporation (E).

City	Bioretention		Permeable Pavement		Green Roof	
	Q/P	E/P	Q/P	E/P	Q/P	E/P
New York City	67%	33%	69%	31%	70%	30%
Miami	70%	30%	74%	26%	75%	25%
Phoenix	26%	74%	42%	58%	40%	60%
San Francisco	82%	18%	86%	14%	84%	16%

For the permeable pavement testbed in San Antonio - Texas of Model Calibration / Validation test, overall, the model performance is acceptable, with better results for simulating large-flow events, assuming no uncertainty in rainfall and observed seepage discharge. The largest errors occurred for low-flow events and in the long-term runoff coefficient, which generated a bias of 27.6% more volume modeled than observed. Despite the overall satisfactory model performance, some systematic discrepancies—particularly in low-flow conditions—can be attributed to both

observational uncertainties and inherent system complexities. The largest mass balance errors were observed during periods of minimal flow, which are especially sensitive to measurement noise and instrumentation thresholds, in particular from the flow meter reference gauging position. Errors in low-flow quantification may arise from limited resolution of flow meters, inaccuracies in the positioning of level sensors, or delayed response of the measurement system. Additionally, uncertainties in rainfall input data—especially in short-duration, low-intensity events—can propagate through the model and lead to significant discrepancies in predicted seepage volumes. These factors combined can partially explain the overestimation of modeled runoff volumes compared to observations.

Furthermore, several physical and numerical limitations influence the model's ability to reproduce observed behavior under real-world conditions. Spatial heterogeneity in the testbed, such as variable compaction or uneven infiltration capacity, may not be fully captured by a 1D model representation. The presence of macropores or preferential flow paths introduces non-uniform flow dynamics that are difficult to replicate without a more detailed spatial structural description. By automatic calibration, however, we estimate effective material properties at the LID scale rather than providing a representative physical description of the parameters.

8.2. Long-term Hydrologic Signatures

Long-term hydrologic behavior of a typical design of permeable asphalts, green roofs, and bioretention systems was evaluated using flow and evaporation duration curves over a 30-year simulation period (1995–2025) for four representative cities: New York City, Miami, Phoenix, and San Francisco. These locations were selected to encompass a wide range of climatic conditions, including humid subtropical, arid desert, and Mediterranean regimes. Duration curves provide a probabilistic view of hydrologic fluxes, enabling a more comprehensive assessment of the frequency, persistence, and magnitude of both runoff and evaporation beyond typical event-based analyses.

Flow duration curves reveal substantial variation across climates. In wetter regions such as Miami and New York City, the system generates frequent surface and subsurface outflows, consistent with high precipitation frequencies and intensities. These curves exhibit steep slopes at higher exceedance probabilities, indicating event-driven responses, but also maintain low-level flows across a range of intermediate percentiles. In contrast, San Francisco and Phoenix demonstrate flatter duration curves with extended periods of negligible outflow, reflecting prolonged dry seasons or drought conditions interspersed with short, high-intensity runoff events.

Evaporation duration curves exhibit similarly distinct patterns. In arid climates, particularly Phoenix, evaporation is persistent and low in magnitude, governed more by high evaporative demand than by water availability. It is important to note that the results presented here focus exclusively on vertical fluxes under non-rainfall conditions, as the model was forced using a net precipitation input (i.e., rainfall minus potential evapotranspiration). This formulation assumes instantaneous evapotranspiration whenever rainfall equals or exceeds atmospheric demand, effectively filtering out periods of active precipitation. As such, the duration curves for evaporation characterize only periods in which rainfall is absent, providing insight into how stored water is depleted through evaporation during dry spells. In contrast, New York and Miami have typical lower potential evapotranspiration/evaporation demand, but presented higher actual fluxes due to water availability in these areas when compared to Phoenix and San Francisco.

In wetter climates, where runoff events occur frequently but are moderate in magnitude, the system effectively attenuates peak flows and reduces total runoff volumes (see Fig. 2 rainfall duration curves compared to the discharge duration curves of Fig. 5). This functionality can alleviate pressure on combined sewer systems and help mitigate urban flooding, especially under future scenarios of intensifying precipitation.

In terms of maximizing proxy groundwater recharge or treated runoff, the simulations indicate that permeable pavements generally achieve the highest fraction of precipitation leaving the system as subsurface discharge across the studied climates, with a particularly clear advantage in arid, water-limited settings such as Phoenix, where they produce the largest recharge and avoid excessive evaporation losses. In winter-wet Mediterranean climates such as San Francisco, all low-impact development practices considered in this study achieve high recharge fractions, with only marginal differences between them. In humid climates such as New York City and Miami, the differences are small, with permeable pavements and green roofs performing slightly better than bioretention systems. The relatively high hydraulic conductivity of permeable pavements promotes large infiltration rates, which may exceed the drainage capacity of underlying soils with poor permeability, potentially leading to perched water tables or seepage. Therefore, permeable pavements are most suitable where subgrade soils or underdrain systems can safely convey the infiltrated water, if the goal is to maximize groundwater recharge. Bioretention systems and green roofs, while sometimes producing lower recharge in arid regions due to higher evaporative losses, provide vegetated surfaces that contribute to habitat creation, microclimate regulation, and urban aesthetics, and may be preferable in locations where these co-benefits are of primary importance or where groundwater recharge must be moderated.

A few successful evaluations of continuous simulation of bioretention systems, permeable pavements, and green roofs are available in the literature (Cipolla et al., 2016; Wang et al., 2019; Brunetti et al., 2016). Empirical evidence of the actual hydrologic performance of these systems for long-term durations, as numerically evaluated in this paper, however, is widely lacking since most studies are often evaluated for relatively short periods varying from months to a few years. The maintenance of these potential hydrologic benefits/performance is contingent on preserving the designed infiltration capacity over time. Sediment accumulation, surface clogging, and biogeochemical transformations within the pore structure can progressively reduce system performance. Without regular maintenance—such as vacuum sweeping, surface cleaning, or periodic rehabilitation—flow and evaporation patterns may deviate significantly from modeled conditions, potentially reverting the system toward conventional impervious behavior. Therefore, understanding long-term hydrologic signatures also reinforces the need for proactive asset management strategies to ensure that infiltration LID systems continue to deliver their intended environmental and hydraulic benefits across decades of service.

8.3. Potential Applications, Limitations, and Uncertainties

The results from the model applications demonstrate its versatility in simulating a wide range of hydrological scenarios, highlighting its generality and potential for application across diverse climatic regions and urban development contexts. A key strength of the model lies in its fully coupled architecture, which integrates variably saturated flow, surface fluxes, and catchment-scale runoff generation within a single framework. This eliminates the need for external hydrological models or pre-processing steps to generate boundary conditions, thereby streamlining the simulation process

and reducing sources of interfacing error. Additionally, the model is implemented in MATLAB, a widely used and accessible programming environment that lowers the barrier for adoption among students, educators, and researchers. While we acknowledge that other programming languages could offer enhanced computational performance, MATLAB was chosen for its code simplicity, readability, and widespread use in academic research and teaching.

As with any computational model describing an incomplete representation of a real-world system, epistemic uncertainty arises when simplifying complex hydrological processes—for example, by reducing a 3D flow system to a 1D approximation and solving Richards' equation. Such simplifications may extend beyond the representative elementary volume (REV), where the assumptions underlying the fundamental equations may no longer hold (Farthing and Ogden, 2017).

Spatial heterogeneity and the presence of preferential flow pathways represent additional sources of epistemic uncertainty that are not fully captured by one-dimensional modeling frameworks (Coutinho et al., 2016). In real-world permeable pavement systems, material properties such as porosity, permeability, and compaction often vary significantly both laterally and vertically due to construction practices, aging, clogging, and uneven loading. These heterogeneities can result in localized zones of enhanced infiltration or hydraulic resistance, thereby promoting non-uniform flow behavior. Moreover, preferential pathways—such as those formed by subsurface cracks, edge effects near curbs, or incomplete material compaction—can cause bypass flow or short-circuiting, leading to faster drainage or uneven saturation profiles (Meng et al., 2020). Such complex flow patterns violate the assumptions of homogeneity and isotropy required by classical formulations of Richards' equation, and may result in over- or under-predictions of infiltration and storage when using lumped or 1D models. While these effects can sometimes be indirectly captured through calibration, determining effective parameter estimations, they remain a critical limitation for predictive modeling and highlight the need for caution when interpreting results or transferring calibrated models across sites with differing subsurface conditions.

Equifinality is a prominent manifestation of epistemic uncertainty in variably saturated flow modeling, particularly in physically based models governed by the Darcy–Richards equation (Beven, 2006). It describes the phenomenon where multiple combinations of model parameters yield similarly acceptable or indistinguishable simulation results, despite having different physical interpretations. This is especially relevant in Richards-based models due to the nonlinear and interdependent behavior of soil hydraulic properties, such as the van Genuchten parameters (α , n), saturated hydraulic conductivity (K_s), and water retention limits (θ_r , θ_s). These parameters often exhibit compensatory behavior—for example, a lower K_s may be offset by a higher α , resulting in comparable infiltration responses under certain boundary conditions (Gomes Jr et al., 2025). As a result, the parameter space becomes non-unique during calibration, making it possible for different parameter sets to replicate observed discharge or soil moisture equally well. This non-uniqueness complicates parameter identifiability, undermines confidence in extrapolated predictions, and presents challenges for inverse modeling. Although automated calibration methods may identify parameter sets that optimize performance metrics such as NSE or KGE, they do not ensure that the selected values accurately represent the underlying physical system. By automatic calibration, however, we estimate effective material properties at the LID scale rather than providing a representative physical description of the parameters. The performance of the derived set of parameters must then be validated against field observations in a different dataset to ensure applicability in real-world conditions (Beven and Young, 2013).

An important limitation of this study lies in the use of daily rainfall and reference evapotranspiration (ET_0) as input forcings for the long-term performance assessment of Model Application. This modeling choice was intentional, as our objective was to capture the long-term hydrologic behavior and seasonal variability of infiltration-based systems rather than short-term, high-intensity events, while still maintaining computational efficiency (Costa et al., 2020). However, using daily time-steps inherently smooths sub-daily rainfall intensities, making it difficult to represent infiltration-excess overland flow and other rapid runoff generation mechanisms (Šimnek and Weihermüller, 2018). In reality, short-duration rainfall bursts—particularly in urban environments—can exceed the infiltration capacity of surface layers, leading to ponding, lateral redistribution, and surface overflow. Under such conditions, additional hydrologic processes beyond bottom exfiltration, including infiltration-excess runoff and temporary surface storage, may play a critical role in system response. These dynamics, including the influence of ponding depth on short-term retention and release, were not explicitly represented in this analysis and are the object of further studies. Nonetheless, the model is equipped to support finer temporal resolution in future applications, allowing users to investigate event-based behavior, surface overflow, and the dynamic interplay between infiltration and surface hydrology when high-resolution data are available.

Another key modeling assumption in this study is that the systems are lined, and only bottom exfiltration is considered as the mechanism for runoff generation. This assumption is appropriate for many typical permeable pavement systems and green roofs, where underdrain capacity exceeds the media's saturated hydraulic conductivity, effectively preventing lateral losses. However, this simplification may not be valid for unlined bioretention systems that are designed to allow lateral exfiltration into surrounding soils. In such cases, subsurface lateral flow could represent a significant component of the water balance, particularly under prolonged wet conditions or in sloped installations. Furthermore, if the local water table rises above the bottom of the bioretention profile, lateral infiltration into the system may occur, introducing reverse flow dynamics that are not captured by the current model formulation. As such, the results presented here should not be interpreted as representative for conditions where significant lateral exchange with the surrounding soil or groundwater system is expected.

9. Conclusions

This study presented a physics-based, fully coupled modeling toolbox for simulating infiltration-based LID systems under continuous, climate-driven conditions. The framework integrates a mixed-form Richards Equation solver with a conceptual rainfall-runoff module and dynamic evapotranspiration representation, supporting long-term analysis of bioretention systems, permeable pavements, and green roofs.

Model performance was verified against Hydrus-1D using four benchmark scenarios: (i) constant pressure infiltration into dry sandy soil, (ii) infiltration into dry clay loam, (iii) capillary rise from a saturated water table, and (iv) uniform rainfall applied as a constant flux. These cases tested the model under both Dirichlet and Neumann boundary conditions, and across coarse to fine-textured soils. The toolbox reproduced pressure head and moisture dynamics with high fidelity (average RMSE for heads and water content of 0.020 m and 0.003), confirming numerical accuracy and robustness across contrasting hydraulic regimes against benchmark model Hydrus-1D.

Validation of the model to a monitored permeable pavement installation in San Antonio, Texas demonstrated its ability to reproduce real-world system behavior under variable rainfall conditions. After calibration, the model achieved strong agreement with observed outflows (calibration: $NSE = 0.94$, $R^2 = 0.95$, validation: $NSE = 0.73$, $R^2 = 0.80$), effectively capturing both the timing and magnitude of drainage responses. While high-flow events were well represented, greater deviations occurred under low-flow conditions, likely due to measurement uncertainty and unmodeled lateral heterogeneity. These results support the model's applicability for assessing infiltration performance and media properties in operational LID systems, while also highlighting the limitations of one-dimensional assumptions under complex site conditions.

Long-term simulations across four U.S. cities revealed distinct hydrologic signatures for each LID system under varying climate regimes. In arid regions such as Phoenix, all systems exhibited high evaporation efficiency (up to 74% of annual precipitation) and minimal runoff, highlighting the dominant role of atmospheric demand in water balance partitioning. In contrast, humid climates such as Miami and New York City showed lower evaporation ratios (25–33%) and consistently higher subsurface discharge, driven by more frequent and intense rainfall. Bioretention and green roof systems demonstrated greater variability in evaporation and runoff responses across climates compared to permeable pavements, which maintained relatively stable behavior due to their relatively lower conductivity and higher water retention when compared to permeable pavements. These findings underscore the importance of climate-responsive design and suggest that optimizing LID performance requires explicit consideration of local hydroclimatic conditions in system selection and sizing.

Despite the model's performance applicability, several limitations remain. The current formulation adopts a one-dimensional vertical flow assumption, which does not capture lateral heterogeneity, preferential pathways, or subsurface exfiltration that may occur in real-world systems. Additionally, the use of daily-scale climate forcing in long-term simulations limits the resolution of short-duration events and precludes detailed analysis of surface ponding or rapid runoff generation, and may overestimate evaporation rates. The absence of snow-related processes further constrains its applicability in cold-climate studies where other runoff mechanisms might be important. However, results indicate that this parsimonious model can provide accurate results, suggesting that most of the main hydrological properties can be achieved with a simple 1D Mixed-Form Richards model.

Future developments will address these limitations by incorporating higher-resolution forcing, lateral and surface flow components, and contaminant fate and transport modules, thereby expanding the model's utility for comprehensive urban hydrologic and water quality assessments. Furthermore, the framework can support the development and testing of real-time control strategies for adaptive LID operation under evolving climate and urbanization conditions. Future work may also explore optimization-based design of LID systems, where media properties and geometric configurations are systematically tuned to match long-term flow duration curves. This approach would enable the design of LID systems that more effectively mimic pre-development hydrologic conditions, thereby supporting more resilient and hydrologically functional urban landscapes.

Acknowledgment

The authors gratefully acknowledge the support by the City of San Antonio under grant SAT0002723.

Appendix A. Supplementary Material

Supplementary data related to this article can be found at https://github.com/marcusnobrega-eng/LID_tool.

Data Availability Statement

Forcing data from Meteostat used for the long-term scenarios is available at: <https://meteostat.net/en/>. Hydrus-1D can be downloaded at <https://www.pc-progress.com/en/Default.aspx?h1d-downloads>. Algorithms and data used are available in an open repository at https://github.com/marcusnobrega-eng/LID_tool.

CRedit authorship contribution statement

Marcus Nóbrega Gomes Jr.: Conceptualization, Methodology, Software, Validation, Formal analysis, Investigation, Data Curation, Writing - Original Draft, Writing - Review Editing, Visualization. **Jose Artur Teixeira Brasil:** Writing - Review Editing, Investigation, Data Curation, Resources. **Drew Johnson:** Writing - Review Editing, Funding acquisition. **Athanassios T. Papagiannakis:** Writing - Review Editing, Funding acquisition. **Marcio Hofheinz Giacomoni:** Writing - Review Editing, Funding acquisition, Visualization, Resources.

References

- Ajirotutu, R.O., Adeyemi, A.B., Ifechukwu, G.O., Iwuanyanwu, O., Ohakawa, T.C., Garba, B.M.P., 2024. Designing policy frameworks for the future: Conceptualizing the integration of green infrastructure into urban development. *Journal of Urban Development Studies* 2.
- Beven, K., 2006. A manifesto for the equifinality thesis. *Journal of hydrology* 320, 18–36.
- Beven, K., Young, P., 2013. A guide to good practice in modeling semantics for authors and referees. *Water Resources Research* 49, 5092–5098.
- Brunetti, G., Šimnek, J., Piro, P., 2016. A comprehensive numerical analysis of the hydraulic behavior of a permeable pavement. *Journal of Hydrology* 540, 1146–1161.
- Chithra, S., Nair, M.H., Amarnath, A., Anjana, N., 2015. Impacts of impervious surfaces on the environment. *International Journal of Engineering Science Invention* 4, 27–31.
- Cipolla, S.S., Maglionico, M., Stojkov, I., 2016. A long-term hydrological modelling of an extensive green roof by means of swmm. *Ecological engineering* 95, 876–887.
- Costa, I.R.d.A., Coutinho, A.P., Montenegro, S.M.G.L., Rabelo, A.E.C.d.G.d.C., Santos, S.M.d., Alves, E.M., Antonino, A.C.D., 2020. Sensitivity of hydrodynamic parameters in the simulation of water transfer processes in a permeable pavement. *RBRH* 25, e47.
- Coutinho, A.P., Lassabatere, L., Montenegro, S., Antonino, A.C.D., Angulo-Jaramillo, R., Cabral, J.J., 2016. Hydraulic characterization and hydrological behaviour of a pilot permeable pavement in an urban centre, brazil. *Hydrological Processes* 30, 4242–4254.
- Dussailant, A.R., Wu, C.H., Potter, K.W., 2004. Richards equation model of a rain garden. *Journal of Hydrologic Engineering* 9, 219–225.
- Farthing, M.W., Ogden, F.L., 2017. Numerical solution of richards' equation: A review of advances and challenges. *Soil Science Society of America Journal* 81, 1257–1269.
- Feddes, R.A., Kowalik, P., Kolinska-Malinka, K., Zaradny, H., 1976. Simulation of field water uptake by plants using a soil water dependent root extraction function. *Journal of Hydrology* 31, 13–26.
- van Genuchten, M.T., 1980. A closed-form equation for predicting the hydraulic conductivity of unsaturated soils. *Soil science society of America journal* 44, 892–898.
- Gomes Jr, M.N., Bauser, H.H., Troch, P.A., 2025. Identifying the state dependence of effective material properties in a simplified hydrologic hillslope model. *Authorea Preprints*.
- Gomes Jr, M.N., Giacomoni, M.H., de Macedo, M.B., do Lago, C.A.F., Brasil, J.A.T., de Oliveira, T.R.P., Mendiondo, E.M., 2023. A modeling framework for bioretention analysis: Assessing the hydrologic performance under system uncertainty. *Journal of Hydrologic Engineering* 28, 04023025.

- Gomes Jr, M.N., Mendiondo, E.M., Dornelles, F., Papagiannakis, A.T., Giacomoni, M.H., 2021. Permeable pavement hydrological model to assess the long-term efficiency of maintenance using high-resolution temperature and rainfall data, in: World Environmental and Water Resources Congress 2021, pp. 1103–1117.
- Hargreaves, G.H., Allen, R.G., 2003. History and evaluation of hargreaves evapotranspiration equation. *Journal of irrigation and drainage engineering* 129, 53–63.
- Hargreaves, G.H., Samani, Z.A., 1982. Estimating potential evapotranspiration. *Journal of the irrigation and Drainage Division* 108, 225–230.
- Huang, J., He, J., Valeo, C., Chu, A., 2016. Temporal evolution modeling of hydraulic and water quality performance of permeable pavements. *Journal of Hydrology* 533, 15–27.
- Li, H., Harvey, J., Ge, Z., 2014. Experimental investigation on evaporation rate for enhancing evaporative cooling effect of permeable pavement materials. *Construction and Building Materials* 65, 367–375.
- Li, Y., Babcock Jr, R.W., 2014. Green roof hydrologic performance and modeling: a review. *Water science and technology* 69, 727–738.
- List, F., Radu, F.A., 2016. A study on iterative methods for solving richards' equation. *Computational Geosciences* 20, 341–353.
- Liu, Y., Li, T., Peng, H., 2018. A new structure of permeable pavement for mitigating urban heat island. *Science of the Total Environment* 634, 1119–1125.
- Batalini de Macedo, M., Gomes Júnior, M.N., Jochelavicius, V., de Oliveira, T.R.P., Mendiondo, E.M., 2022a. Modular design of bioretention systems for sustainable stormwater management under drivers of urbanization and climate change. *Sustainability* 14, 6799.
- Batalini de Macedo, M., Nobrega Gomes Junior, M., Pereira de Oliveira, T.R., H. Giacomoni, M., Imani, M., Zhang, K., Ambrogi Ferreira do Lago, C., Mendiondo, E.M., 2022b. Low impact development practices in the context of united nations sustainable development goals: A new concept, lessons learned and challenges. *Critical Reviews in Environmental Science and Technology* 52, 2538–2581.
- McClymont, K., Cunha, D.G.F., Maidment, C., Ashagre, B., Vasconcelos, A.F., de Macedo, M.B., Dos Santos, M.F.N., Júnior, M.N.G., Mendiondo, E.M., Barbassa, A.P., et al., 2020. Towards urban resilience through sustainable drainage systems: A multi-objective optimisation problem. *Journal of Environmental Management* 275, 111173.
- McGrane, S.J., 2016. Impacts of urbanisation on hydrological and water quality dynamics, and urban water management: a review. *Hydrological Sciences Journal* 61, 2295–2311.
- Meng, A., Tan, Y., Xing, C., Lv, H., Xiao, S., 2020. Investigation on preferential path of fluid flow by using topological network model of permeable asphalt mixture. *Construction and Building Materials* 242, 118163.
- Nash, J.E., Sutcliffe, J.V., 1970. River flow forecasting through conceptual models part i—a discussion of principles. *Journal of hydrology* 10, 282–290.
- Olszewski, J.M., Davis, A.P., 2013. Comparing the hydrologic performance of a bioretention cell with predevelopment values. *Journal of Irrigation and Drainage Engineering* 139, 124–130.
- Pons, V., Abdalla, E.M.H., Tscheikner-Gratl, F., Alfredsen, K., Sivertsen, E., Bertrand-Krajewski, J.L., Muthanna, T.M., 2023. Practice makes the model: A critical review of stormwater green infrastructure modelling practice. *Water Research* 236, 119958.
- Pugliese, F., Gerundo, C., De Paola, F., Caroppi, G., Giugni, M., 2022. Enhancing the urban resilience to flood risk through a decision support tool for the lid-bmps optimal design. *Water Resources Management* 36, 5633–5654.
- Rahman, A.S., Šimnek, J., Bradford, S.A., Ajami, H., Meles, M.B., Chen, L., Szymkiewicz, A., Pawlowicz, M., Triana, J.S.A., Trasvina, J.A.C., et al., 2025. A new externally coupled, physically-based multi-model framework for simulating subsurface and overland flow hydrological processes on hillslopes. *Journal of Hydrology* , 133842.
- Richards, L.A., 1931. Capillary conduction of liquids through porous mediums. *Physics* 1, 318–333.
- Rossman, L.A., et al., 2010. Storm water management model user's manual, version 5.0. National Risk Management Research Laboratory, Office of Research and . . .
- Roy-Poirier, A., Champagne, P., Filion, Y., 2010. Review of bioretention system research and design: past, present, and future. *Journal of Environmental Engineering* 136, 878–889.
- Šimnek, J., Weiermüller, L., 2018. Using hydrus-1d to simulate infiltration .
- Simunek, J., Van Genuchten, M.T., Sejna, M., 2005. The hydrus-1d software package for simulating the one-dimensional movement of water, heat, and multiple solutes in variably-saturated media. *University of California-Riverside Research Reports* 3, 1–240.
- Skaggs, R.W., Youssef, M., Chescheir, G., 2012. Drainmod: Model use, calibration, and validation. *Transactions of the ASABE* 55, 1509–1522.
- Wang, J., Chua, L.H., Shanahan, P., 2019. Hydrological modeling and field validation of a bioretention basin. *Journal of environmental management* 240, 149–159.
- Wasko, C., Nathan, R., Stein, L., O'Shea, D., 2021. Evidence of shorter more extreme rainfalls and increased flood variability under climate change. *Journal of Hydrology* 603, 126994.
- Westra, S., Fowler, H.J., Evans, J.P., Alexander, L.V., Berg, P., Johnson, F., Kendon, E.J., Lenderink, G., Roberts, N., 2014. Future changes to the intensity and frequency of short-duration extreme rainfall. *Reviews of geophysics* 52, 522–555.
- Zhou, Q., Leng, G., Su, J., Ren, Y., 2019. Comparison of urbanization and climate change impacts on urban flood volumes: Importance of urban planning and drainage adaptation. *Science of the Total Environment* 658, 24–33.